EXAFS studies on undercooled liquid $Co_{80}Pd_{20}$ alloy

G. Jacobs and I. Egry
Institut für Raumsimulation, Deutsches Zentrum für Luft- und Raumfahrt e.V., D-51170 Köln, Germany
(Received 5 June 1998; revised manuscript received 11 September 1998)

By combining electromagnetic levitation with the EXAFS method it is possible to investigate the short-range order of metallic melts in a wide temperature range. Due to the containerless environment it is even possible to obtain insight into the metastable state of a deeply undercooled melt not amenable by other methods. This allows us to study the solid and the liquid state in the same temperature range. Here we report on the first quantitative EXAFS measurements on a liquid $Co_{80}Pd_{20}$ alloy undercooled by more than 300 °C, and on solid $Co_{80}Pd_{20}$. From the spectra, we have obtained the temperature dependence of the neighbor distances as well as of the Debye-Waller factors. [S0163-1829(99)10905-6]

I. INTRODUCTION

Research on the structure of metallic melts is difficult for many reasons: Metals are not transparent to visible light, so that x rays or neutron sources are necessary to yield insight into the material. In addition, the melting temperature of most metals is very high, which leads to problems of finding a crucible material resisting high temperatures and not reacting with the sample.

The electromagnetic levitation technique is an elegant method for containerless processing of metallic melts. Using radio-frequency, inhomogeneous electromagnetic fields, it provides heating and positioning for electrically conducting materials. The sample levitates inside a coil and can be probed by several noncontact diagnostic tools, as described in, e.g., Ref. 1. Due to the extremely pure conditions it is possible to undercool the levitating melt several 100 °C below the melting temperature and access this metastable state. The potential of this method and experiments on undercooled melts are discussed in Ref. 2.

In the absence of any long-range order in the melt, structural studies can be performed with methods that are sensitive to the short-range order in the sample. The EXAFS (extended x-ray absorption fine structure) analysis provides element-specific information about the neighbor distance, the Debye-Waller factor, and the coordination number.[3] Pioneering EXAFS measurements on low melting liquid Zn above the melting temperature were published by Crozier and Seary in 1980,[4] where they studied the effect of the asymmetric pair distribution on the analysis of EXAFS spectra. More recently, EXAFS was applied to high-temperature melts.[5] Since the EXAFS technique, being an absorption experiment, is barely affected by an ill-defined experimental geometry (due to the sample's motion), it seemed possible to combine both levitation and EXAFS for structural studies of undercooled metallic melts.

The first EXAFS experiments on levitated, undercooled metallic melts at the Hamburger Synchrotronstrahlungslabor (HASYLAB) of the Deutsches Elektronensynchrotron (DESY) showed the feasibility[6] of this combination. Here we report on the first quantitative analysis of EXAFS spectra of undercooled Co-Pd alloys.

The binary alloy Co-Pd has a simple phase diagram: it is fully miscible at all compositions and does not possess any intermetallic phases. Furthermore, it can be easily undercooled below the hypercooling limit.[7]

At the composition Co–20 at. % Pd, it shows a minimum between liquidus and Curie temperature, and ferromagnetic properties of the undercooled melt have been reported.[8] Therefore, $Co_{80}Pd_{20}$ was chosen as a model system for the present study. Making use of the fact that we could compare the short-range order in the solid and in the liquid phase at the same temperature over a wide temperature range, we could clearly separate temperature effects from structural effects. Similar experiments have been previously performed on undercooled liquid germanium, using an emulsion technique.[9] In germanium, however, the solid-liquid phase transition coincides with an insulator-metal transition, which makes the interpretation of the observed effects more difficult. In addition to clarifying the fundamental difference between the liquid and the solid state, we have also studied quantitatively the structural contributions to the macroscopic thermal expansion.

II. EXPERIMENTAL DETAILS

A. EXAFS

The x-ray absorption coefficient of an isolated atom exhibits sharp edges at distinct energies. These energies correspond to the ionization thresholds of the core electrons. If the atom is embedded in condensed matter, the absorption coefficient is observed to oscillate up to energies of about 1000 eV above the absorption edge. This oscillation is called EXAFS (extended x-ray absorption fine structure) and is caused by the scattering of the emitted photoelectron by the surrounding atoms. A comprehensive review of EXAFS can be found in the book by Teo.[10]

The EXAFS signal $\chi(k)$ is defined as the normalized deviation of the absorption coefficient $\mu(k)$ of the condensed matter from its value for an isolated atom $\mu_0(k)$:

$$\chi(k)=\frac{\mu(k)-\mu_0(k)}{\mu_0(k)}, \tag{2.1}$$

where k is the wave vector of the emitted photoelectron. If E_0 denotes the energy of the absorption edge and m the

electron rest mass, then k is related to the energy of the incident x-ray energy E by

$$E-E_0=\frac{\hbar^2k^2}{2m}. \tag{2.2}$$

In scattering theory, using plane-wave and single-scattering approximations, $\chi(k)$ is given by

$$\chi(k)=\frac{|f(k)|}{k}\int_0^\infty \frac{p(r)}{r^2}e^{-2r/\lambda(k)}\sin[2kr+\phi(k)]dr, \tag{2.3}$$

where $|f(k)|$ and ϕ are the characteristic backscattering amplitude and phase shift due to the scattering of the neighbor atoms, $\lambda(k)$ is the mean free path of the photoelectron, and $p(r)$ is the bond length probability density, which is proportional to the pair-distribution function $g(r)$. In the case of small disorder in the system a Gaussian probability density with variance σ is assumed and Eq. (2.3) leads to

$$\chi(k)=-\sum_j \frac{N_j}{r_j^2k}\ |f_j(k)|\ \ e^{-2\sigma_j^2k^2}e^{-2r_j/\lambda_j(k)} \times\sin[2kr_j+\phi_j(k)]. \tag{2.4}$$

Here N_j is the number of neighbors of type j in the jth shell with distance r_j from the central atom, $f_j(k)$ and $\phi_j(k)$ are the characteristic scattering amplitude and phase shift due to the scattering at an atom of type j and $\exp[-2\sigma_j^2k^2]$ is the Debye-Waller factor.

For disordered systems, like glasses, melts, or crystals at high temperatures, the assumption of a symmetric pair-distribution function is no longer correct, since the back-scattering atoms feel the anharmonicity of the pair potential. For that reason the pair-distribution function of these systems will become asymmetric.

For the analysis of our EXAFS spectra the GNXAS method of Filipponi *et al.*[11] is used. This method, like other advanced methods for the EXAFS analysis, does not use the plane-wave approximation and takes into account mutiple-scattering effects, which are not considered in Eq. (2.4). It allows a decomposition of the measured x-ray absorption signal (XAS) into contributions of the n-body distribution function $g_n(r)$ (GN). Filipponi and Di Cicco[9] and D' Angelo *et al.*[12] developed the following asymmetric model function:

$$p(r)=\frac{2}{\sigma|\beta|\Gamma(q)}\left(q+\frac{2(r-R)}{\sigma\beta}\right)^{q-1}\exp\left[-\left(q+\frac{2(r-R)}{\sigma\beta}\right)\right] \tag{2.5}$$

with Euler's gamma function $\Gamma(q)$ and $q=4/\beta^2$. The distribution depends on three parameters: The expectation value of the atomic distance R, the variance of the distribution σ, and an asymmetry parameter $\beta=K_3/\sigma^3$, where K_3 is the third cumulant of the distribution. In the small β limit Eq. (2.5) can be described by a Gaussian distribution.

Inserting the model distribution function, Eq. (2.5), into the general EXAFS formula, Eq. (2.3), a model EXAFS for a given radial distribution can be calculated, and vice versa. From the fits, R, σ, and β can be determined as functions of temperature.

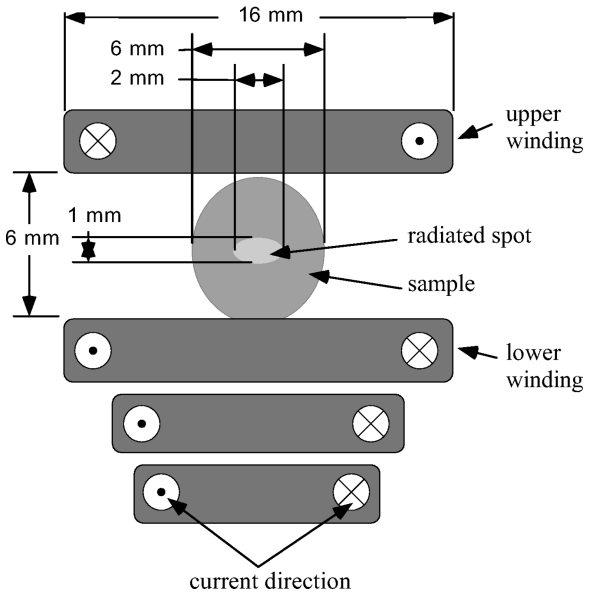

FIG. 1. Scale sketch of the levitated sample in the coil, seen in the direction of the incident beam.

B. Electromagnetic levitation

Electrically conducting materials can be processed without a container by using the electromagnetic levitation technique. If a sample is placed into a high-frequency alternating inhomogeneous electromagnetic field **B**, eddy currents are induced within the sample. These currents will interact with the field leading to levitation of the sample caused by the Lorentz force **F**, which is proportional to the gradient of the field. Simultaneously the sample is heated due to Ohmic losses of the induced currents. The power absorbed by the sample is proportional to the square of the field strength. If the energy loss due to radiation and heat conduction is lower than the power absorption, the sample can finally be molten. For further details on the electromagnetic levitation see, e.g., the review by Herlach *et al.*[1]

Since the potential generated by the levitation coil is only very shallow, the sample is not fixed within the coil, but performs oscillations about its equilibrium position. These translational oscillations have typical amplitudes in the range of a few millimeters and a frequency of a few Hz. At the same time the liquid sample will perform surface oscillations with a frequency in the order of 40 Hz. For recording of sufficiently smooth EXAFS spectra both oscillations have to be suppressed as much as possible by using a suitable levitation coil.

C. Experimental setup and implementation

The experiments were carried out at the European Synchrotron Radiation Facility (ESRF) in Grenoble, France, at Beamline 18 (BM 29). The levitation chamber is aligned to the beam in such a way that the levitated sample is illuminated symmetrically to its equator. The levitation coil has an inner diameter of about 16 mm and a gap of about 6 mm between the lower and upper windings, which allows free observation of the sample from the side for the x-ray beam as well as for the detectors. A scale sketch of the sample in the levitation coil is shown in Fig. 1. The dimensions of the

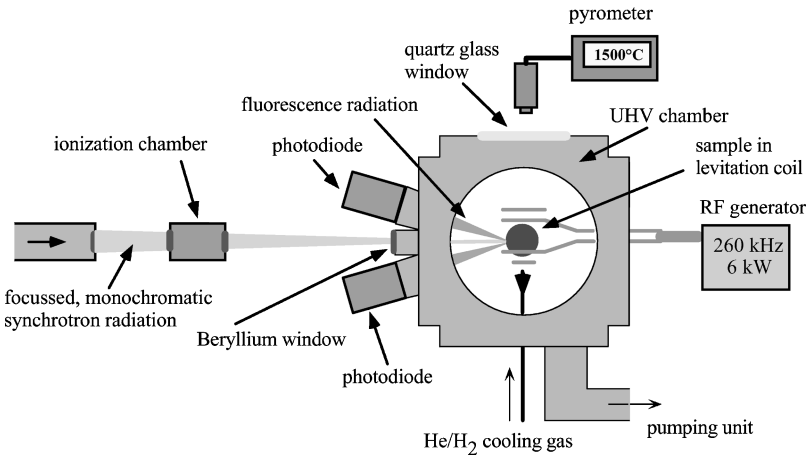

FIG. 2. Experimental setup: The monochromatic synchrotron radiation reaches the levitating sample after passing an ionization chamber. The secondary fluorescence radiation is detected by four photodiodes, which are placed concentrically around the incident beam. For clarity the sketch does not show the horizontal pair of diodes.

beam are carefully chosen to make sure that it is always focused onto the sample surface. Such an adjustment suppresses the influence of sample translations on the absorption spectra. Using samples of 5–6 mm diameter, a beam size of 1 mm height and 2 mm width leads to an optimized result.

Before the experiment the sample is placed into a vacuum chamber (Fig. 2), which is evacuated to a pressure better than 10^{-5} mbar to prevent the sample from being contaminated by atmospheric oxygen and to reach maximum undercoolability. For the experiment the chamber is filled with a 96% He and 4% H_2 mixture of high purity up to a pressure of about 1.2 bars. This reducing atmosphere avoids the formation of oxides on the sample surface that could lead to premature nucleation. The temperature of the sample is measured with a pyrometer and is adjusted by convective cooling with an electropneumatically controlled gas flow for keeping the temperature constant during the measurement.

After passing an ionization chamber for measuring the incident beam intensity, the beam enters the levitation chamber through a thin beryllium window. The thickness of the sample does not allow one to measure the absorption directly in transmission, so we measure the fluorescence radiation of the transition of an electron from the L to the K state. To minimize the influence of the sample movement on the spectra, a horizontal and a vertical pair of photodiodes is used, which are placed concentrically in backward direction (about 16°) around the incident beam.

The measurements were done at the cobalt K edge ($E_0 = 7.709$ keV) in the energy range from 7.6 keV to 8.3 keV. In the region above the edge the energy points were chosen to be equidistant in k space using a step width of $\Delta k = 0.05$ Å^{-1}. With an integration time of 5 sec per energy point for the levitating melt, one spectrum was obtained in about 35 min. During this time it was necessary to maintain the sample liquid at a constant temperature, which limits the range of accessible undercooling because the nucleation rate increases exponentially with undercooling.[1]

For quantitative analysis of the EXAFS of the melt, averaged spectra from four single spectra at constant temperature were used to further reduce the influence of the sample movement.

The measurements on the solid sample at room temperature were performed using the same facility with the levitation field switched off and with identical samples (spheres of 5–6 mm diameter) supported by an Al_2O_3 sample holder. In contrast to that, the measurements on the solid samples at elevated temperatures were performed using a special high-temperature furnace,[13] that allows the heating of the sample up to the solidus temperature. A flat sample with a thickness of about 100 μm was prepared. For direct heating of the sample, an electric dc current was fed through the sample. The direction of the incident synchrotron beam was normal to the sample's surface, and the fluorescence radiation was detected nearly in the backward direction.

The self-absorption of all samples was taken into account by using the correction of Tröger *et al.*[14]

III. RESULTS AND DISCUSSION

A. EXAFS spectra

Figure 3 shows k-weighted EXAFS spectra of solid $Co_{80}Pd_{20}$ at room temperature and at 850 °C with the least-squares fit including contributions up to the third shell. The damping of the amplitude at high temperatures is evident.

The k-weighted EXAFS spectra of liquid $Co_{80}Pd_{20}$ are shown in Fig. 4. It was possible to obtain spectra at temperatures more than 210 °C above the liquidus temperature [$T_l(Co_{80}Pd_{20}) = 1337$ °C] as well as at an undercooling of more than 310 °C. The spectra at the highest temperatures are more noisy because of the decreasing sample stability with increasing temperature. On the other hand, for measuring the EXAFS at 1020 °C it was necessary to choose an integration time of only 2 sec per energy point to keep the sample liquid during the measurement, so that the averaging over the sample movement is not very good. Comparing the low noise spectra from $T = 1400$ °C down to $T = 1050$ °C a distinct increase of the EXAFS with decreasing temperature is clearly visible: At lower temperatures the EXAFS amplitude rises and a fourth maximum around $k = 8.5$ Å^{-1} becomes more pronounced. According to Fig. 3 (note the different ordinate scales) it is obvious that the EXAFS is much more distinctive in the solid than in the melt.

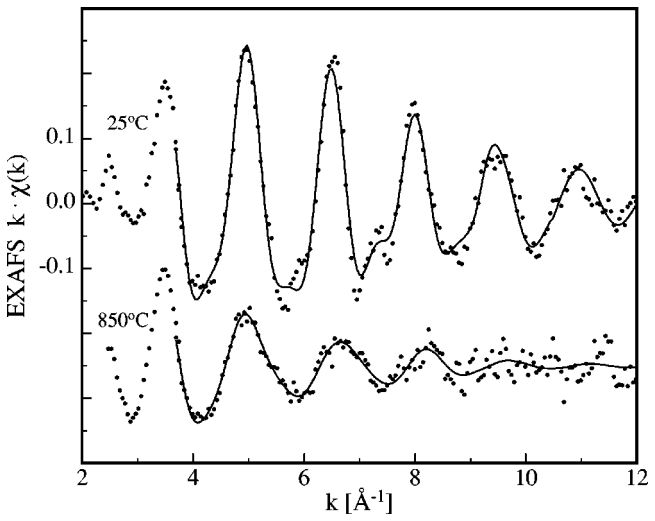

FIG. 3. Experimental, *k*-weighted EXAFS spectra of solid $Co_{80}Pd_{20}$ at 25 °C and 850 °C. The solid line is a least-squares fit to the experimental data including contributions up to the third shell. The spectra are shifted on the ordinate scale.

Comparing the signal-to-noise ratio from the stably positioned crystal with the levitated melt shows the effectiveness of our procedure of averaging over the sample motion.

The Fourier transforms $\chi(r)$ of the EXAFS spectra for the solid and liquid sample are shown in Figs. 5 and 6, respectively. To obtain $\chi(r)$, the k range from 3.5 to 10.0 Å^{-1} was used and weighted with k^2. From Eq. (2.3) it is obvious that $\chi(r)$ is related to the pair correlation function $g(r)$.

Figure 5 shows $\chi(r)$ for the solid at 25 °C and 850 °C. At both temperatures, there is the main peak around 2.5 Å, corresponding to the nearest-neighbor distance. Also, there exist at least four additional maxima. The height of the main peak decreases by a factor of 5 as the temperature is raised from 25 °C to 850 °C.

In Fig. 6, $\chi(r)$ is shown for the liquid sample in the temperature range from 1050 °C to 1550 °C. The maximum

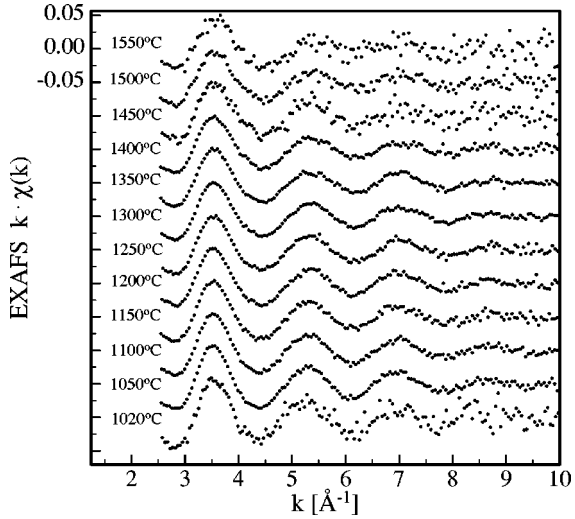

FIG. 4. Experimental, *k*-weighted EXAFS spectra of liquid $Co_{80}Pd_{20}$ in the temperature range from 1550 °C to 1020 °C. The spectra are shifted on the ordinate scale.

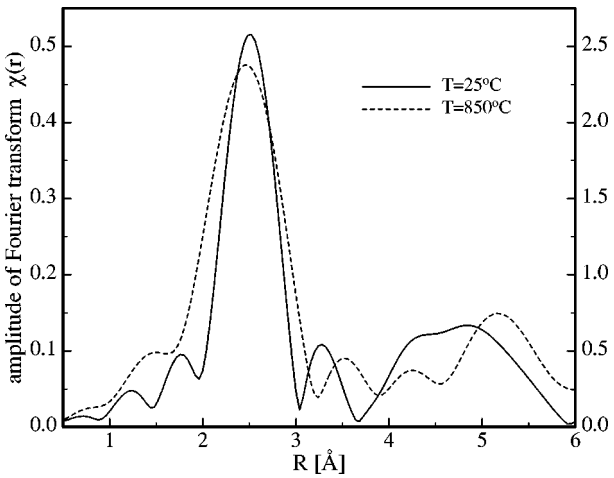

FIG. 5. Fourier transform $\chi(r)$ of the experimental EXAFS spectra of solid $Co_{80}Pd_{20}$ at 25 °C (solid line, right ordinate) and at 850 °C (dotted line, left ordinate). Note that the amplitude of the high-temperature spectrum is smaller by a factor of 5.

corresponding to nearest neighbors is present at all temperatures, whereas, in contrast to the solid, maxima related to more distant neighbors are washed out. The peak height of the liquid at 1050 °C is reduced by a factor of 2 as compared to the solid at 850 °C. However, the half width of the peak is nearly the same for these two temperatures, indicating that the Debye-Waller factor is dominated by temperature effects. From Fig. 6 it is evident that an increase in temperature leads to a reduction and broadening of the peak. In summary, the short-range order extending to the nearest neighbors is maintained in the liquid whereas medium-range order related to more distant neighbors is characteristic of the solid state. The behavior of the short-range order will be discussed in the following in terms of neighbor distance and Debye-Waller factor.

B. Fitting procedure

With the GNXAS method it is possible to calculate model backscattering signals for each component directly in *k* space

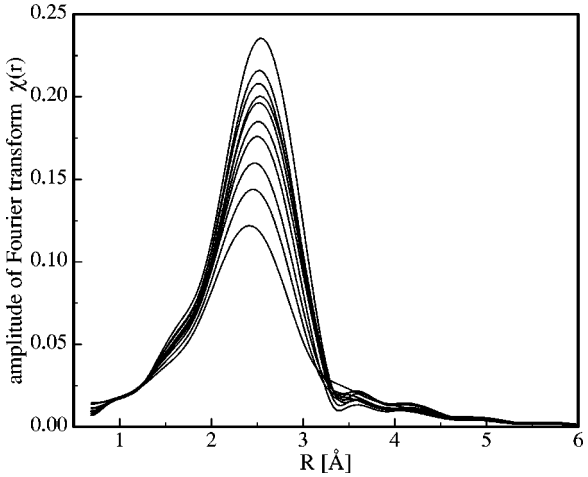

FIG. 6. Fourier transform $\chi(r)$ of the experimental EXAFS spectra of liquid $Co_{80}Pd_{20}$ in the temperature range from 1550 °C (lowest curve) to 1050 °C (highest curve) in steps of 50 °C.

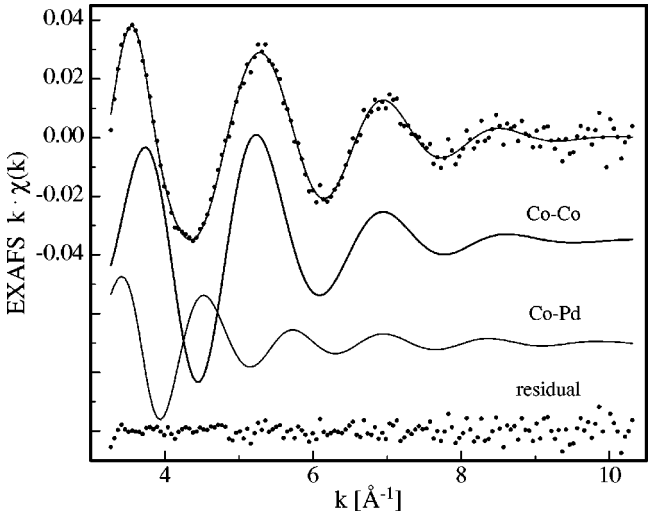

FIG. 7. EXAFS of liquid $Co_{80}Pd_{20}$ at 1050 °C: Data and fit with asymmetric pair-distribution functions for the first cobalt and palladium shell and the residual.

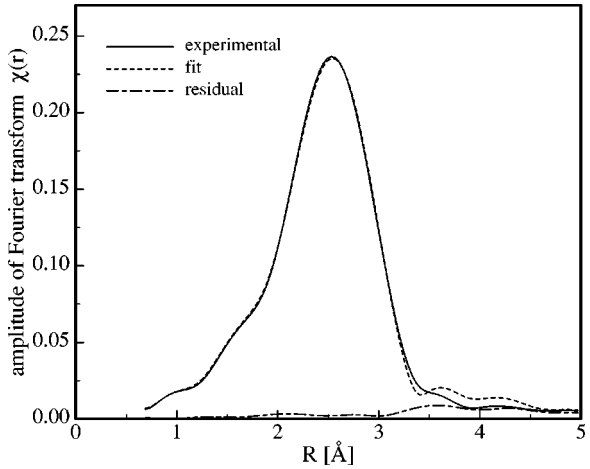

FIG. 8. EXAFS of liquid $Co_{80}Pd_{20}$ at 1050 °C: Fourier transform of data, fit, and residual.

and to perform a least-squares fit to the experimental spectra without any filtering. For the analysis of our spectra, we assumed a face-centered cubic (fcc) structure of the crystal and an icosahedral structure in the melt. The model was fitted to the measured spectra assuming 80% cobalt and 20% palladium around the absorbing cobalt atom for all temperatures. As parameters we varied the threshold energy E_0 [cf. Eq. (2.2)], both neighbor distances $R_{Co\text{-}Co}$ and $R_{Co\text{-}Pd}$ and their variances $\sigma_{Co\text{-}Co}$ and $\sigma_{Co\text{-}Pd}$, as well as the total coordination number and the asymmetry parameter β. The threshold energy was found to be $E_0 = 7720 \pm 2$ eV for all temperatures. In order to reduce the number of fitting parameters we decided to fix β for the liquid spectra to its value of 0.5 that was obtained from the spectrum at 1300 °C.

In Fig. 7 the decomposition of the measured EXAFS of liquid $Co_{80}Pd_{20}$ at 1050 °C into contributions from the first cobalt and palladium shell is shown. The topmost curve represents the measured data points with the total fit. In the *k*-weighted spectrum the oscillation is clearly visible up to the fourth maximum which is at $k = 8.5$ Å^{-1}. Beneath, the contributions of the cobalt and of the palladium neighbors are plotted separately. The longer wavelength for the cobalt backscatterer is obvious, denoting a shorter distance for the cobalt neighbors. The residual describes the difference between the model and the data points and is a measure for the quality of the fit. The lack of any structure in the residual indicates the agreement between the data and our fit.

The Fourier transform of the data, the fit, and the residual is shown in Fig. 8. The shape of the main peak is well described by the fit.

C. Neighbor distance

Figure 9 shows the temperature dependence of the effective neighbor distance of liquid and solid $Co_{80}Pd_{20}$ in comparison. At room temperature the distance between the cobalt atoms and between cobalt and palladium atoms was evaluated to be $R_{Co\text{-}Co}(25\,°C) = 2.51 \pm 0.01$ Å and $R_{Co\text{-}Pd}(25\,°C) = 2.56 \pm 0.02$ Å, respectively. The nearest-neighbor Co-Co distance in this alloy is essentially the same as in pure cobalt (hcp) with lattice parameters $a = 2.505 \pm 0.009$ Å and $c = 4.065 \pm 0.009$ Å (e.g,. Ref. 15). During heating of the crystal both neighbor distances increase slightly with increasing temperature while the difference of the distances remains relatively small due to the presence of the crystal lattice.

On melting, the effective Co-Co distance reduces drastically in contrast to the Co-Pd distance that rises slightly from its value for the high-temperature crystal. Both distances remain nearly temperature independent over the whole temperature range of more than 500 °C and no difference between the normal liquid and the metastable undercooled melt can be seen. It is well known that an increasing asymmetry of the pair-distribution function can lead to an apparent decrease of the neighbor distances as seen by EXAFS (e.g., Crozier and Seary[4]). In our analysis, we allow for an asymmetric distribution, but we have to keep the skewness parameter β constant, due to convergence problems. Therefore, we cannot rule out that the reduction of the effective Co-Co distance on melting is due to an increasing skewness of the

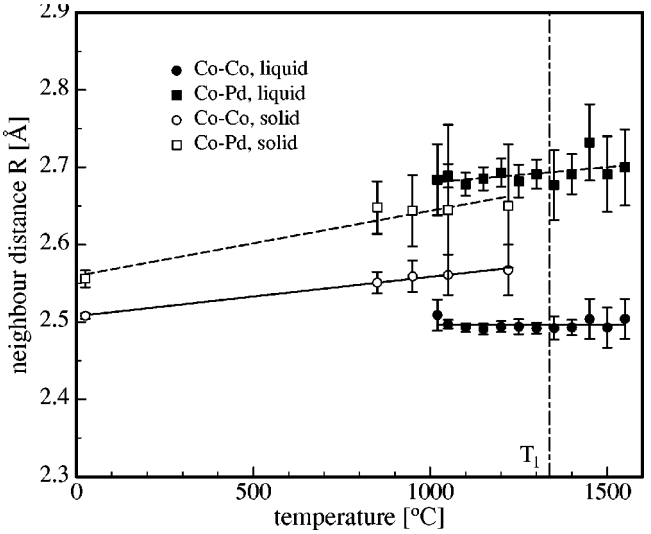

FIG. 9. Distance of the first cobalt and palladium shell from the central cobalt atom in liquid and solid $Co_{80}Pd_{20}$. T_l marks the liquidus temperature.

TABLE I. Temperature dependence of the distance of the first cobalt and palladium shell from the central cobalt atom in solid and liquid $Co_{80}Pd_{20}$.

	Solid $R[T\ (°C)]$ (Å)	Liquid $R[T\ (°C)]$ (Å)
Co shell: $R_{Co\text{-}Co}$	$2.51+5.1\times10^{-5}\ T$	$2.50-0.01\times10^{-5}\ (T-1337)$
Pd shell: $R_{Co\text{-}Pd}$	$2.56+8.4\times10^{-5}\ T$	$2.69+4.02\times10^{-5}\ (T-1337)$

distribution. On the other hand, the observed behavior is consistent with a hard-sphere model for the liquid. Using tabulated values (e.g., Kittel[16]) for the ionic radius of cobalt ($R_{ion}=1.25$ Å) and palladium ($R_{ion}=1.38$ Å), the difference between the solid and the liquid at the same temperature can easily be explained. In the liquid the neighbor distances are determined mainly by the radii of the participating ions. Increasing the temperature leads only to an increase of the amplitude of the atomic vibration (see below) that leaves the expectation value of the distance unchanged. This means that the thermal expansion of the melt cannot be explained by an increase of the interatomic distances.

Table I summarizes the results for the temperature dependence of the neighbor distances in solid and liquid $Co_{80}Pd_{20}$.

D. Debye-Waller factor

In Fig. 10, the temperature dependence of the variance of both distances in liquid and solid $Co_{80}Pd_{20}$ is shown. The contribution of vibrations to the Debye-Waller factor can be adequately described by a simple Einstein model[17] with an appropriately chosen frequency. In this model the vibrational contribution σ_{vib} to the variance in a diatomic system is given by[10]

$$\sigma_{vib}^2 \cong \frac{T}{\mu}\left(\frac{4.836c}{\nu}\right)^2. \tag{3.1}$$

Here μ denotes the reduced mass of the system, ν the vibrational frequency, and c the speed of light. It is obvious that according to this model the vibrational contributions to the variance scale like the reciprocal reduced masses of the constituents. Using tabulated values for the masses ($m_{Co}=58.93$ amu and $m_{Pd}=106.4$ amu) and for the phonon frequency $\nu(Co_{80}Pd_{20})=6.9$ THz, e.g., Ref. 18) the contribution can be calculated and yields $\sigma^2_{Co\text{-}Co,vib}=0.0048$ Å^2 and $\sigma^2_{Co\text{-}Pd,vib}=0.0038$ Å^2 at room temperature. This is in excellent agreement with the experimental data (see Table II).

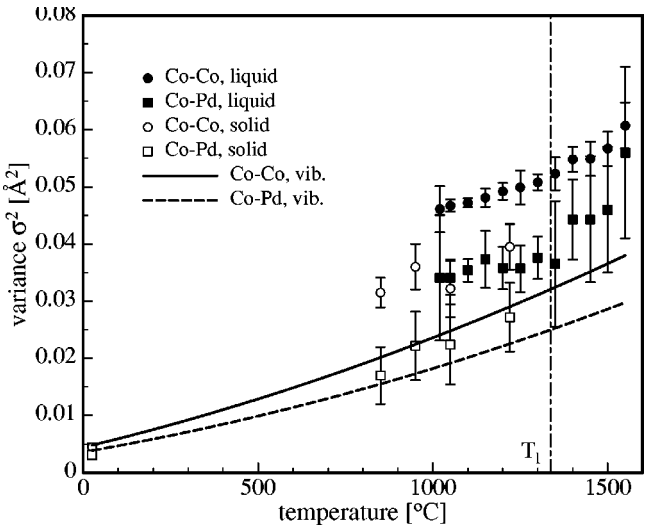

FIG. 10. Variance of the distance of the first cobalt and palladium shell from the central cobalt atom in liquid and solid $Co_{80}Pd_{20}$ in comparison with the vibrational contribution according to the Einstein model. T_l marks the liquidus temperature.

Upon heating of the crystal, the variances increase stronger than is predicted by the Einstein model. The difference cannot be explained by the temperature dependence of the phonon frequency, but is due to increasing structural disorder in the sample. Such disorder could be caused by an increasing number and size of defects. On melting, the variances rise discontinuously. It is tempting to attribute this rise to the onset of diffusion in the liquid, giving rise to additional disorder. However, the slope of the experimental values of the variances in the melt is nearly identical to the slope predicted by the Einstein model, which means that the temperature dependence of the variances is dominated by atomic vibrations, even in the liquid.

Table II summarizes the temperature dependence of the variances of the nearest-neighbor distances in the crystal and in the melt evaluated by linear regression of the data points.

E. Thermal expansion

According to a method suggested by Newville and Stern[19] it is possible to use an anharmonic effective potential $U(r)$ of the form

$$U(r)=\frac{1}{2}a(r-R_0)^2+b(r-R_0)^3+c(r-R_0)^4, \tag{3.2}$$

with the constants a, b, and c, to calculate the thermal volume expansion α_V caused by the anharmonicity of the pair potential. It is given by

$$\alpha_V \cong 3\frac{k_B(a-3R_0b)}{R_0^2a^2}. \tag{3.3}$$

The pair-distribution function related to the potential given in Eq. (3.2) can be approximately calculated using $g_{cal}=\exp[-U(r)/k_BT]$. This relationship is valid in the very low density limit only.[20] We use it as a simple way to parametrize our pair-distribution function and to derive the thermal expansion from Eq. (3.3), not for a derivation of the pair potential. Of course, the use of this relationship at the densities considered here is a potential source for (quantitative) errors. By fitting this calculated function to the experimental distribution function, Eq. (2.5), it is possible to evaluate the constants a, b, and c yielding a thermal volume expansion of $\alpha\approx0.6\times10^{-4}$ K^{-1}.

TABLE II. Temperature dependence of the variance of the first cobalt and palladium shell from the central cobalt atom in solid and liquid $Co_{80}Pd_{20}$.

	Solid σ^2 [T (°C)]($Å^2$)	Liquid σ^2 [T (°C)] ($Å^2$)
Co shell: $\sigma^2_{Co\text{-}Co}$	$0.0045+2.9\times10^{-5}\ T$	$0.053+2.5\times10^{-5}\ (T-1337)$
Pd shell: $\sigma^2_{Co\text{-}Pd}$	$0.0031+2.0\times10^{-5}\ T$	$0.041+2.6\times10^{-5}\ (T-1337)$

Using the literature values[21] for the density of liquid cobalt [$\rho_{Co}(T)=7.75$—$10.9\times10^{-4}(T-1768\ \text{K})\ \text{g/cm}^3$] and liquid palladium [$\rho_{Pd}(T)=10.49$—$12.3\times10^{-4}(T-1827\ \text{K})\ \text{g/cm}^3$], the density of the alloy can be calculated according to Crawley:[22]

$$\rho=\frac{\sum x_iA_i}{V_M}, \tag{3.4}$$

where V_M is the molar volume, A_i the atomic weight, and x_i is the concentration of component i in the alloy.

This leads to a volume expansion coefficient of $\alpha_V\approx1.2\times10^{-4}\ \text{K}^{-1}$, which was verified by a direct measurement[23] of the thermal expansion. Therefore, we conclude that the temperature dependence of interatomic distances and Debye-Waller factors accounts for only about 50% of the macroscopic thermal expansion. The missing 50% can be due to the formation of vacancies in the liquid that should become evident as a decrease in coordination number. This is consistent with our experimental results and with the conventional interpretation that thermal expansion in liquids is caused by a decrease in coordination number rather than by an increase in nearest-neighbor distance.[24] Unfortunately, it is a systematic weakness of EXAFS that it is rather inaccurate in yielding coordination numbers. Therefore, the missing 50% could equally well be due to an increasing skewness of the distribution with temperature, which we did not consider in our analysis. Auxilliary information from diffraction experiments is required to improve the accuracy and to confirm our assertion.

IV. CONCLUSION

The combination of the electromagnetic levitation technique with the EXAFS method allows one to investigate the short-range order of metallic melts in a wide temperature range including deep undercooling. Using this combination it was possible for the first time to compare the structure of the solid and the liquid phase of macroscopic samples over a wide temperature range, in our experiments over more than 200 °C.

By using a proper procedure for averaging over the unavoidable sample motion it is possible to obtain meaningful spectra that can be analyzed applying an asymmetric pair-distribution function. With the GNXAS method, the structural parameters for the components can be evaluated separately, which was done for the environment of the cobalt atoms in $Co_{80}Pd_{20}$.

It could be seen that neighbor distances in the melt are dominated by the ionic radii of the components and are nearly temperature independent. Similarly, the atomic distances in the crystal do not differ much from their room temperature values even close to the melting point.

For the solid at room temperature the variances can be described by the Einstein model for harmonic oscillations neglecting disorder. The temperature dependence of the variances in the melt is similar to those in the solid. We argued that this behavior may be due to a superposition of temperature-dependent atomic vibrations and a temperature-independent structural disorder.

It was shown that the increasing amplitude of the atomic vibrations in the melt is not sufficient to explain the thermal expansion of the sample, indicating that there is another important contribution to the thermal expansion of liquids from either the reduction of the coordination number with increasing temperature or an increasing skewness.

ACKNOWLEDGMENT

We would like to thank the BM29 staff from ESRF, especially A. Filipponi for his support during the measurements on the levitating samples and for performing the high-temperature measurements on the solid sample.

[1] D. M. Herlach, R. F. Cochrane, I. Egry, H. J. Fecht, and A. L. Greer, Int. Mater. Rev. **38**, 273 (1993).

[2] *Undercooled Metallic Melts: Properties, Solidification and Metastable Phases*, Proceedings of a NATO Advanced Research Workshop, June 6–12, 1993 Il Ciocco, Italy, edited by D. M. Herlach, I. Egry, P. Baeri, F. Spaepen [Mater. Sci. and Eng. A **178**, 1–313 (1994)].

[3] *X-ray Absorption: Principles, Applications, Techniques of EXAFS, SEXAFS, and XANES*, edited by D. C. Koningsberger and R. Prins (Wiley, New York, 1988).

[4] E. D. Crozier, and A. J. Seary, Can. J. Phys. **58**, 1388 (1980).

[5] A. di Cicco and A. Filipponi, J. Non-Cryst. Solids **205-207**, 304 (1996).

[6] G. Jacobs, I. Egry, K. Maier, D. Platzek, J. Reske, and R. Frahm, Rev. Sci. Instrum. **67**, 3683 (1996).

[7] T. Volkmann, G. Wilde, R. Willnecker, and D. M. Herlach, J. Appl. Phys. **83**, 3028 (1998).

[8] D. Platzek, C. Notthoff, D. M. Herlach, G. Jacobs, D. Herlach, and K. Maier, Appl. Phys. Lett. **65**, 1723 (1994).

[9] A. Filipponi and A. Di Cicco, Phys. Rev. B **51**, 12 322 (1995).

[10] B. K. Teo, in *EXAFS Spectra*, edited by B. K. Teo and D. C. Joy (Plenum, New York, 1981).

[11] A. Filipponi, A. Di Cicco, and C. R. Natoli, Phys. Rev. B **52**, 15 122 (1995).

[12] P. D'Angelo, A. Di Nola, A. Filipponi, N. V. Pavel, and

D. Roccatano, J. Chem. Phys. **100**, 985 (1994).
[13] A. Filipponi and A. Di Cicco, Nucl. Instrum. Methods Phys. Res. B **93**, 302 (1994).
[14] L. Tröger, D. Arvanitis, K. Baberschke, H. Michaelis, U. Grimm, and E. Zschech, Phys. Rev. B **46**, 3283 (1992).
[15] *Smithells Metals Reference Book*, edited by E. A. Brandes (Butterworths, London, 1983).
[16] C. Kittel, *Introduction to Solid State Physics*, (Wiley, New York, 1987).
[17] E. Sevillano, H. Meuth, and J. J. Rehr, Phys. Rev. B **20**, 4908 (1979).
[18] *Zahlenwerte und Funktionen aus Naturwissenschaften und Technik*, edited by K. H. Hellwege, Landolt-Börnstein, New Series, Group III, Vol. 13, pt. a (Springer, Berlin, 1981).
[19] M. Newville and E. A. Stern (unpublished).
[20] J. P. Hansen and I. R. McDonald, *Theory of Simple Liquids* (Academic Press, London, 1986).
[21] T. Iida and R. I. L. Guthrie, *The Properties of Liquid Metals* (Clarendon Press, Oxford, 1993).
[22] A. F. Crawley, Int. Metall. Rev. **19**, 32 (1974).
[23] M. Langen and G. Jacobs (unpublished).
[24] S. Takeuchi, Mater. Trans., JIM **30**, 647 (1989).